Article

Not peer-reviewed version

# Automatic Morphological Evaluation Using Three-Dimensional Transeophageal Echocardiography of Patients with Mitral Prolapse and Insufficiency: Comparison with Patients Without Cardiac Chambers Alterations

Marcelo L C Vieira *, Ana C T Rodrigues, Edgar Daminelo, Adriana Reche, Gustavo P de Almeida, Alessandra J Oliveira, Luiz O A Santos, Rafael B Piveta, Rodrigo A C Meirelles, Cláudia G Monaco, Fernando C Oliveira, Fernando A Solis, Wercules Oliveira, Alessandro C Lianza, Adriana Sanudo, Edgar B Lira Filho, Sérgio A F Curcio, Robinson Poffo, Cláudio H Fischer, Samira S Morhy

Posted Date: 6 January 2026

doi: 10.20944/preprints202601.0344.v1

Keywords: mitral insufficiency; valvular heart disease; three-dimensional echocardiography; artificial intelligence

*Article*

# Automatic Morphological Evaluation Using Three-Dimensional Transeophageal Echocardiography of Patients with Mitral Prolapse and Insufficiency: Comparison with Patients Without Cardiac Chambers Alterations

**Marcelo L C Vieira [1,2], Ana C T Rodrigues [1], Edgar Daminelo [1], Adriana Reche [1], Gustavo P de Almeida [1], Alessandra J Oliveira [1], Luiz O A Santos [1], Rafael B Piveta [1], Rodrigo A C Meirelles [1], Cláudia G Monaco [1], Fernando C Oliveira [1], Fernando A Solis [1], Wercules Oliveira [1], Alessandro C Lianza [1], Adriana Sanudo [3], Edgar B Lira Filho [1], Sérgio A F Curcio [1], Robinson Poffo [1], Cláudio H Fischer [1,3] and Samira S Morhy [1]**

[1] Hospital Israelita Albert Einstein, Sao Paulo, Brazil
[2] Heart Institute (InCor), Sao Paulo, Brazil
[3] São Paulo Federal University (UNIFESP), Sao Paulo, Brazil
* Correspondence: mluiz766@terra.com.br; Tel: +55 11 981888301

**Abstract**

**Background:** There is paucity of information concerning automatic mitral valve apparatus analysis of patients with mitral valve prolapse (MVP). **Objectives:** We aimed to study with an automatic three-dimensional transesophageal echocardiography (TEE) dedicated software patients with moderate and severe mitral regurgitation when compared to patients with no structural cardiac chamber alterations (patients with patent foramen ovale (PFO) who underwent TEE) . **Methods:** We employed a TEE software dedicated to automatic analysis of 34 parameters of the mitral valve apparatus comparing MVP patients with moderate and severe mitral regurgitation and patients with PFO without cardiac chamber structural alterations. Mitral valve effective regurgitant orifice (ERO) and regurgitant volume were correlated to automatic MVP parameters. **Results:** 59 MVP patients and 43 PFO patients were analysed. All MVP patients presented P2 mitral valve prolapse, 15 (25.4% ) with both posterior and anterior prolapse. Twenty-seven automatic parameters (79%) were different concerning MVP and PFO patients ($p<0.05$): diameters, area, perimeter, height, angle, coaptation width, lenght, closure line lenght, annulus. ERO was 0.43 $\pm$ 0.11 cm2 , and regurgitant volume: 62.2 $\pm$ 14.9 ml/beat. Automatic analysis correlated to 75 percentile ERO MVP patients (ERO> 0.48 $cm^2$): Posterior Leafltet Area (r:0.74, p:0.031); Posterior Leafltet Lenght (r:0.73, p:0.032); Tenting area (r:0,41, p:0.048**). Conclusions:** Automatic mitral valve parameters analysis were different concerning MVP and no structural cardiac chamber (PFO) patients. 75 percentile ERO MVP patients (ERO> 0.48 $cm^2$) correlated to posterior leaflet parameters.This anatomic information could be useful to planning and surgical treatment of mitral valve prolapse patients.

**Keywords:** mitral insufficiency; valvular heart disease; three-dimensional echocardiography; artificial intelligence

## 1. Introduction

Mitral valve regurgitation caused by mitral valve prolapse presents clinical relevance due to its high prevalence in clinical practice [1–13]. Mitral valve apparatus consists of a complex group of structures such as valve cusps, the set of chordae that fix and traction the cusps, the mitral valve annulus, the papillary muscles that insert into the ventricular wall, and the ultrastructural and

 doi:10.20944/preprints202601.0344.v1



contiguous relationship with the left ventricle and left atrium [1–13]. Each of these elements has its own characteristics and particular aspects which make the mitral valve apparatus very unique.

A better understanding of the structures that make up the mitral valve allows us to determine the best time for surgical or percutaneous intervention [1–13]. Imaging methods for the geometric and functional analysis of heart disease have evolved rapidly with the development of computing, nanotechnology, and artificial intelligence. For the analysis of valvular heart disease, echocardiography occupies a prominent position due to its ability to demonstrate cardiac anatomy with great accuracy and proximity to anatomical reality.[1–13]. In the 21st century, we have the opportunity to rapidly demonstrate cardiac structures using transesophageal echocardiography and artificial intelligence from multiple spatial planes, taking into account multiplanar three-dimensional analysis, in real time, with the aid of algorithms specifically designed for demonstrating the mitral valve apparatus

Thus, we planned a study to determine the different elements that make up the mitral valve apparatus, the morphofunctional analysis of the structures related to the valve apparatus (left atrium, left ventricle), using a three-dimensional transesophageal echocardiography automatic algorithm dedicated to the analysis of the mitral valve apparatus, (Figures 1 and 2) when compared to patients without structural cardiac chamber changes.

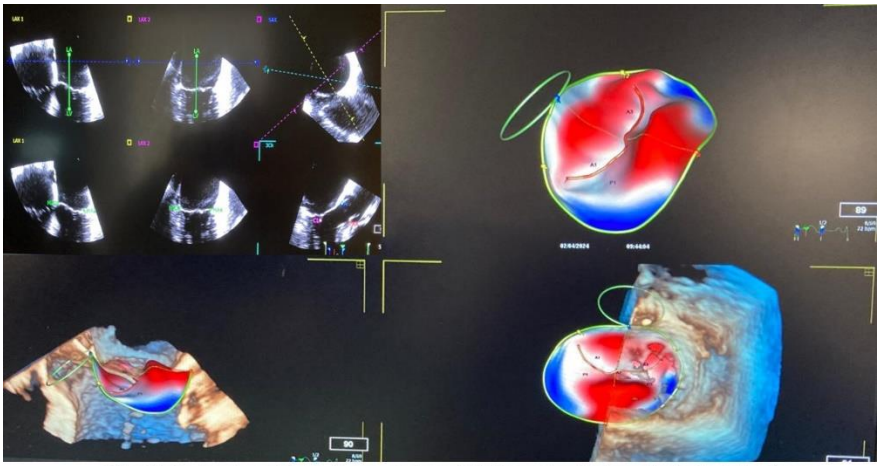


**Figure 1.** Mitral valve prolapse patient. Demonstration of the imaging with the transesophageal tridimensional automatic dedicated software. Superior left image: different planes for apparatus reconstruction. Other images (in red): demonstration of different segments with mitral valve prolapse in different views.

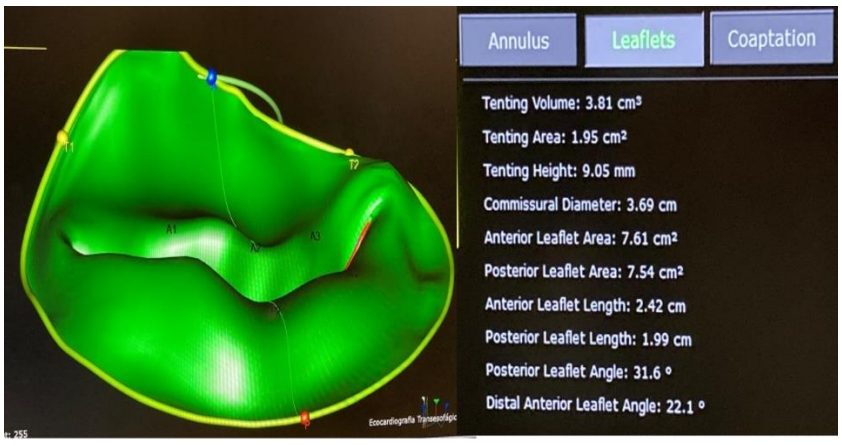


**Figure 2.** Mitral valve prolapse patient. Demonstration of different mitral valve apparatus variables measured with the automatic software. Mitral valve in green (atrial view).

 doi:10.20944/preprints202601.0344.v1



## 2. Methods

### *2.1. Patients*

#### 2.1.1. Study Design

A single-center from a Brazilian tertiary hospital centre, prospective study from February 2023 to December 2024 evaluating transesophageal three-dimensional echocardiographic variables with a mitral valve automatic analysis algorithm was performed in 59 consecutive patients with mitral valve regurgitation (grade 2 and 3) due to mitral valve prolapse and 43 patients without structural cardiac chamber alterations who went to echocardiographic examination due to patent oval forame. The study was performed in accordance with the principles established by the Declaration of Helsinki, and the project was approved by the Research Ethics Committee of the hospital. **"Informed consent was obtained from all subjects involved in the study."**

#### 2.1.2. Inclusion Criteria

- Consecutive patients with moderate to severe mitral valve regurgitation, resulting from valve prolapse in analysis for structural treatment.
- Consecutive patients with clinical suspicion of PFO.
- Patients with age over 18 years of age.
-Signed informed consent form to participate in the study.

#### 2.1.3. Exclusion Criteria

- Atrial fibrillation or tachyarrhythmia with hemodynamic instability.
- Presence of significant aortic insufficiency, significant aortic stenosis, or significant mitral stenosis.

### *2.2. Echocardiography*

#### Imaging Acquisition

The images were acquired using a Philips Healthcare Epiq CVx echocardiography device by different investigators of the study, available in the Echocardiography Department of the Hospital. Images were acquired during a conventional transesophageal echocardiographic examination using conventional two-dimensional projections, with analysis of the complex mitral valve apparatus, including detailed analysis of all its components: annulus, cusps, commissures, chordae, papillary muscles, and left ventricle. The projections used for image acquisition were: midesophageal commissural, long-axis, two-chamber, and four-chamber views with and without anteroflexion of the probe; and transgastric short-axis and long-axis views. After the 2D evaluation, 3D acquisitions were obtained in 3D zoom and full-volume formats. 3D zoom images). Repeated 3D zoom images of the mitral valve complex were taken from the atrial aspect corresponding to the surgical view, reducing the overall gain and increasing the magnitude of the selected image.Such acquisitions consist of obtaining subvolumes with angle and temporal resolution greater than the 3D zoom format with a higher volume rate, higher than 25 Hz, coupled to the electrocardiogram in consecutive cardiac cycles, and digitally stored for later analysis of the processed images.

Conventional 2D echocardiographic and Doppler parameters were measured, as follow: left ventricle anteroposterior diameters; RV: right ventricle diastolic diameter short axis diameter; LVEF: Left ventricule ejection fraction (Teicholz method); LA: left atrium anteroposterior diameter and volume; PSAP: pulmonary artery systolic pressure, following previously published international recommendations[16].

 doi:10.20944/preprints202601.0344.v1



*2.3. Imaging Analysis*

The images extracted from the three-dimensional transesophageal study were evaluated using Philips Health Care's artificial automatic software dedicated to the analysis of the mitral valve apparatus (MVA), which is part of Philips Health Care's QLAB software, version 15.0.0. The analysis was performed offline on a workstation by two researchers involved in the investigation.

Echocardiographic variables to be analyzed with artificial intelligence software dedicated to the analysis with three-dimensional transesophageal echocardiography of the elements of the mitral valve apparatus in patients with mitral regurgitation and in patients with patent foramen ovale: mitral annulus anteroposterior diameter (AP Diameter), mitral annulus anterolateral-posteromedial diameter (AL-PM Diameter), sphericity Index (AP / AL-PM), intertrigonal distance, commissural diameter, saddle shaped annulus Area (3D), saddle shaped annulus perimeter (3D), D-shaped annulus area (2D), D-shaped annulus perimeter, annulus height, non-planar angle, tenting volume, coaptation depth, tenting area, angle aortic (AAo-AP), maximum prolapse height, maximal open coaptation gap, maximal open coaptation width, total open coaptation area (3D), anterior leaflet area, posterior leaflet area, distal anterior leaflet angle, posterior leaflet angle, anterior leaflet length, posterior leaflet length, annulus area (2D), anterior closure line length (2D), anterior closure line length (3D), posterior closure line length (2D), posterior closure line length (3D), C-shaped annulus, annular displacement (max), annular displacement velocity (max), tenting volume fraction, annulus area fraction (2D) (Figures 1 and 2).

*2.4. Statistics*

Normally distributed quantitative variables were expressed as mean ± standard deviation or as median and interquartile range (IQR: P25–P75) when not normally distributed; qualitative variables were summarized as number and percentage. The comparison between etiologies (MI and PFO) was performed using Student's t-test for quantitative variables that were normally distributed. For those that were not normally distributed, the Mann-Whitney test was used. For data from participants with MI, Pearson's correlation coefficient (r) and its 95% confidence interval (95% CI) were calculated between the variables ERO and Regurgitant Volume, as well as a scatterplot between the two variables. The Pearson correlation coefficient and its 95% CI were also calculated between each of the variables in the new software and ERO and Regurgitant Volume. When correlation values were $p<0.20$, simple linear regression models were adjusted, thus obtaining the coefficient of explanation ($R^2$) for each of the adjusted models. To adjust a multiple linear regression model, we first assessed the presence of multicollinearity among the variables obtained via the new software, and then selected which variables would be introduced into the multiple linear regression model.

The ERO and Regurgitant Volume variables were categorized based on the 75th percentile of each distribution. Each of the variables obtained via the new software was compared according to the ERO and Regurgitant Volume variable groups. The Student's t-test was applied, and the effect size was calculated using Cohen's test when the variables were normally distributed; otherwise, the Mann-Whitney test was applied, and the effect size was calculated using Cliff's δ. The effect size magnitudes obtained via Cohen's d were interpreted as: trivial (<0.20), small (0.20–0.49), moderate (0.50–0.79), and large (≥0.80). The magnitudes obtained via Cliff's δ were interpreted as: trivial (<0.15), small (0.15–0.32), moderate (0.33–0.46), and large (≥0.47). All analyses were performed in StataNow/MP 19.5 (StataCorp, College Station, TX, USA) and results with p-values less than 0.05 were considered significant. Intra- and inter-observer variability (ICC= Intraclass correlation coefficient) were tested in 15 patients from MVP and PFO groups by the same operator and by a second operator 10 months after the first acquisition.

## 3. Results

The distribution of demographic data according to etiology, echocardiogram measurements according to etiology, comparison of new automatic software measures between etiologies,

 doi:10.20944/preprints202601.0344.v1



descriptive measures of effective regurgitant orifice and regurgitant volume among patients with mitral valve prolapse, new automatic software measures according to 75 percentile of ERO, new automatic software measures according to 75 percentile of regurgitant volume are depicted in Tables 1–6.

**Table 1.** Distribution of demographic data according to etiology.

| Variable | Total (n=102) | Etiology | | p-Value |
|---|---|---|---|---|
| | | MVP (n=59) | PFO (n=43) | |
| **Sex** | | | | **0.001** |
| Female | 43 (42.2) | 17 (28.8) | 26 (60.5) | |
| Male | 59 (57.8) | 42 (71.2) | 17 (39.5) | |
| **Age**, years | | | | **0.006** |
| Mean ± SD | 57,2 ± 18.1 | 61.4 ± 17.2 | 51.5 ± 18 | |
| **Weight**, Kg | | | | 0,123 |
| Mean ± SD | 74.4 ± 15.1 | 76.4 ± 16.1 | 71.7 ± 13.4 | |
| **BMI**, Kg/m$^2$ | | | | 0,232 |
| Mean ± SD | 25.4 ± 3,8 | 25.8 ± 4.2 | 24.9 ± 3.2 | |
| **Body surface**, m$^2$ | | | | 0.134 |
| Mean ± SD | 1.86 ± 0.23 | 1.89 ± 0.25 | 1.82 ± 0.20 | |

MVP: mitral valve prolapse. PFO: patent foramen ovale; SD: standard deviation; Kg: kilogram; BMI: Body Mass Index.

**Table 2.** Echocardiographic measurements according to etiology.

| Variable | Total (n=102) | Etiology | | p-Value |
|---|---|---|---|---|
| | | MVP (n=59) | PFO (n=43) | |
| **LV diastolic diameter** , mm | | | | **<0.001** |
| Mean ± SD | 50.4 ± 7.4 | 53.8 ± 7.1 | 45.6 ± 4.7 | |
| **Septum diastolic diameter**, mm | | | | **<0.001** |
| Mean ± SD | 9.6 ± 1.,7 | 10.2 ± 1.6 | 8.8 ± 1.7 | |
| **Posterior wall diastolic diameter**, mm | | | | **<0.001** |
| Mean ± SD | 9.3 ± 1.5 | 9.8 ± 1.3 | 8.6 ± 1.4 | |
| **RV diastolic diameter**, mm | | | | 0.808 |
| Mean ± SD | 25.2 ± 3.4 | 25.5 ± 3.4 | 25.1 ± 3.3 | |
| **LVEF**, % | | | | **0.030** |
| Mean ± SD | 61.8 ± 8 | 60.4 ± 9.9 | 63.6 ± 3.8 | |
| **LA anteroposterio diameter**, mm | | | | **<0.001** |
| Mean ± SD | 40.7 ± 8.3 | 45.4 ± 7.2 | 34.3 ± 4.8 | |
| **LA Volume**, ml | | | | **<0.001** |
| Mean ± SD | 42.9 ± 16.8 | 51,5 ± 16,8 | 31 ± 6 | |
| **PSAP**, mm Hg | | | | **<0.001** |
| Mean ± SD | 31.9 ± 12.9 | 34.9 ± 13.8 | 24.1 ± 4.7 | |

MVP: mitral valve prolapse. PFO: patent foramen ovale; LV: left ventricle; RV: right ventricle; LVEF: Left ventricule ejection fraction (Teicholz method); LA: left atrium; PSAP: pulmonary artery systolic pressure.

**Table 3.** Comparison of new automatic software measures between etiologies.

| Variable | Etiology | | Difference (IC95%) | Hedges' g (IC95%) | p-Value |
|---|---|---|---|---|---|
| | MVP | PFO | | | |

 doi:10.20944/preprints202601.0344.v1



| | (n=59) | (n=43) | | | |
|---|---|---|---|---|---|
| **AP Diameter** | 4.15 ± 0.47 | 3.48 ± 0.31 | 0.67 (0.52 a 0.83) | 1.62 (1.17 a 2.08) | **<0.001** |
| **AL-PM_Diameter** | 4.43 ± 0.61 | 3.57 ± 0.29 | 0.86 (0.68 a 1.04) | 1.72 (1.26 a 2.17) | **<0.001** |
| **Sphericity_Index (AP / AL-PM)** | 0.94 ± 0.06 | 0.98 ± 0.06 | -0.04 (-0.07 a -0.02) | -0.69 (-1.08 a -0.31) | **<0.001** |
| **Commissural_Diameter** | 4.33 ± 0.58 | 3.36 ± 0.28 | 0.97 (0.80 a 1.14) | 2.01 (1.53 a 2.50) | **<0.001** |
| **Saddle_Shaped_Annulus_Area (3D)** | 15.0 ± 3.5 (n=56) | 10.4 ± 1.6 (n=42) | 4.6 (3.5 a 5.6) | 1.56 (1.10 a 2.02) | **<0.001** |
| **Saddle_Shaped_Annulus_Perimeter (3D)** | 14.2 ± 1.7 (n=55) | 11.9 ± 0.9 (n=42) | 2.3 (1.8 a 2.9) | 1.68 (1.21 a 2.15) | **<0.001** |
| **D-Shaped_Annulus_Area (2D)** | 13.3 ± 3.3 (n=54) | 8.8 ± 1.5 (n=42) | 4.5 (3.5 a 5.5) | 1.70 (1.23 a 2.17) | **<0.001** |
| **D-Shaped_Annulus_Perimeter** | 13.2 ± 2.1 (n=54) | 11.0 ± 0.9 (n=42) | 2.2 (1.6 a 2.9) | 1.34 (0.89 a 1.78) | **<0.001** |
| **Annulus_Height** | 1.00 ± 0.25 | 0.91 ± 0.20 | 0.09 (0.01 a 0.18) | 0.41 (0.01 a 0.80) | **0.044** |
| **Non-planar_Angle** | 143.9 ± 11.5 | 135.7 ± 9.7 | 8.2 (4.0 a 12.3) | 0.75 (0.34 a 1.16) | **<0.001** |
| **Tenting_Volume** Mediana (P25 – P75) | 2.45 (1.59 – 3.83) (n=36) | 3.37 (2.85 – 3.37) (n=42) | -0.85 (-1.59 a -0.11) | -0.76 (-1.41 a 0.05) | **0.039** |
| **Coaptation_Depht** | 9.3 ± 5.2 (n=56) | 11.1 ± 2.4 (n=42) | -1.8 (-3.4 a -0.3) | -0.44 (-0.83 a -0.04) | **0.020** |
| **Tenting_Area** | 1.66 ± 0.94 (n=51) | 1.99 ± 0.62 (n=43) | -0.33 (-0.66 a 0.00) | -0.40 (-0.81 a 0.00) | 0.052 |
| **Angle_Aao-AP** | 112.5 ± 10.2 | 115.6 ± 8.4 | -3.1 (-6.8 a 0.5) | -0.33 (-0.72 a 0.06) | 0.104 |
| **Maximum_Prolapse_Height** Mediana (P25 – P75) | 7.19 (3.61 – 8.86) (n=54) | 1.04 (1.04 – 2.26) (n=41) | 5.91 (4.29 a 7.53) | 4.22 (2.69 a 6.40) | **<0.001** |
| **Maximal_Open_Coaptaiton_Gap** Mediana (P25 – P75) | 2.11 (0 – 3.91) (n=17) | 0.00 (0 – 1.88) (n=10) | 2.11 (-0.54 a 4.76) | 0.53 (0.00 a 2.62) | 0.184 |
| **Maximal_Open_Coaptation_Width** | 42.4 ± 7.8 (n=54) | 32.1 ± 2.9 (n=40) | 10.3 (8.0 a 12.6) | 1.63 (1.16 a 2.11) | **<0.001** |
| **Total_Open_Coaptation_Area (3D)** Mediana (P25 – P75) | 0.19 (0 – 0.54) (n=17) | 0.00 (0 – 0.24) (n=10) | 0.19 (-0.25 a 0.63) | 0.08 (0.00 a 0.45) | 0.225 |
| **Anterior_Leaflet_Area** | 8.92 ± 2.32 (n=59) | 6.10 ± 1.90 (n=42) | 2.82 (1.99 a 3.66) | 1.30 (0.86 a 1.73) | **<0.001** |
| **Posterior_Leaflet_Area** | 10.64 ± 3.26 (n=59) | 7.38 ± 4.20 (n=42) | 3.26 (1.71 a 4.80) | 0.88 (0.46 a 1.29) | **<0.001** |
| **Distal_Anterior_Leaflet_Angle** | 19.8 ± 10.8 (n=59) | 28.1 ± 6.4 (n=41) | -8.3 (-11.7 a -4.8) | -0.89 (-1.26 a -0.51) | **<0.001** |
| **Posterior_Leaflet _Angle** | 29.0 ± 18.4 (n=59) | 38.4 ± 11.9 (n=41) | -9.4 (-15.4 a -3.4) | -0.58 (-0.97 a -0.19) | **0.005** |

 doi:10.20944/preprints202601.0344.v1



| | | | | | |
|---|---|---|---|---|---|
| **Anterior_Leaflet_Lenght** | 2.93 ± 0.48 (n=58) | 2.54 ± 0.56 (n=42) | 0.39 (0.17 a 0.60) | 0.74 (0.33 a 1.15) | **<0.001** |
| **Posterio_Leaflte_Lenght** | 2.52 ± 0.55 (n=59) | 1.96 ± 0.45 (n=42) | 0.56 (0.37 a 0.76) | 1.09 (0.67 a 1.52) | **<0.001** |
| **Annulus_Area (2D)** | 14.5 ± 3.6 (n=58) | 9.9 ± 1.6 (n=42) | 4.6 (3.5 a 5.6) | 1.54 (1.09 a 1.99) | **<0.001** |
| **Anterior_Closure_Line_Lenght (2D)** | 4.08 ± 0.70 (n=57) | 3.08 ± 0.26 (n=41) | 1.00 (0.80 a 1.21) | 1.77 (1.29 a 2.24) | **<0.001** |
| **Anterior_Closure_Line_Lenght (3D)** | 4.26 ± 0.75 (n=57) | 3.17 ± 0.29 (n=41) | 1.09 (0.86 a 1.30) | 1.77 (1.30 a 2.25) | **<0.001** |
| **Posterior_Closure_Line_Lenght (2D)** | 4.08 ± 0.70 (n=57) | 3.08 ± 0.26 (n=41) | 1.00 (0.80 a 1.20) | 1.78 (1.30 a 2.25) | **<0.001** |
| **Posterior_Closure_Line_Lenght (3D)** | 4.25 ± 0.74 (n=57) | 3.30 ± 0.84 (n=41) | 0.95 (0.62 a 1.27) | 1.21 (0.77 a 1.64) | **<0.001** |
| **C-Shaped_Annulus** | 10.37 ± 1.34 (n=57) | 8.34 ± 0.89 (n=42) | 2.03 (1.58 a 2.47) | 1.72 (1.25 a 2.18) | **<0.001** |
| **Annular_Displacement (max)** | 9.8 ± 2.6 (n=57) | 10.2 ± 1.8 (n=41) | -0.4 (-1.3 a 0.5) | -0.18 (-0.58 a 0.22) | 0.384 |
| **Annular_Displacement_Velocity (max)** | 35.3 ± 9.0 (n=9) | 57.0 ± 20.9 (n=6) | -21.7 (-43.7 a 0.3) | -1.38 (-2.27 a -0.50) | 0.052 |
| **Tenting_Volume_Fraction** | 55.6 ± 24.2 (n=24) | 65.3 ± 23.7 (n=40) | -9.7 (-22.2 a 2.8) | -0.40 (-0.90 a 0.10) | 0.121 |
| **Annulus_Area_Fraction (2D)** Median (P25 – P75) | 7.7 (4.0 – 17.2) (n=53) | 14.3 (9.1 – 27.7) (n=42) | -6.9 (-14.1 a 0.25) | -7.10 (-10.80 a -1.50) | **0.006** |

A-P: anteroposterior; AL-PM: anteroposterior-posteromedial.

**Table 4.** Descriptive measures of effective regurgitant orifice and regurgitant volume among patients with mitral valve prolapse.

| | ERO (cm²) | Regurgitant Volume (ml/beat) |
|---|---|---|
| **Mean** | 0.43 | 62.9 |
| **SD** | 0.11 | 14.2 |
| **Median** | 0.42 | 64 |
| **P25** | 0.35 | 54 |
| **P75** | 0.48 | 70 |
| **Minimum** | 0.20 | 30 |
| **Maximum** | 0.77 | 115 |

ERO: effective regurgitant orifice; mL: mililiter; P25: percentile 25: P75: percentile 75; SD: standard deviation.

**Table 5.** New automatic software measures according to 75 percentile of effective regurgitant orifice (ERO).

| Variable | Total (n=51) | ERO | | p-Value | Effect Size # |
|---|---|---|---|---|---|
| | | ≥0.48cm² (n=12) | <0.48cm² (n=39) | | |
| **AP Diameter** | | | | | |
| Mean ± SD | 4.21 ± 0.46 | 4.35 ± 0.46 | 4.17 ± 0.46 | 0.223 | 0.41 |
| **AL-PM_Diameter** | | | | | |
| Mean ± SD | 4.49 ± 0.58 | 4.70 ± 0.64 | 4.42 ± 0.56 | 0.147 | 0.49 |
| **Sphericity_Index (AP / AL-PM)** | | | | | |
| Mean ± SD | 0.94 ± 0.06 | 0.93 ± 0.06 | 0.95 ± 0.07 | 0.461 | 0.47 |
| **Commissural_Diameter** | | | | | |

 doi:10.20944/preprints202601.0344.v1



| | | | | | |
|---|---|---|---|---|---|
| Mean ± SD | 4.37 ± 0.60 | 4.58 ± 0.68 | 4.30 ± 0.56 | 0.160 | 0.47 |
| **Saddle_Shaped_Annulus_Area (3D)** | (n=48) | (n=10) | (n=38) | | |
| Mean ± SD | 15.3 ± 3.6 | 15.9 ± 4.0 | 15.1 ± 3.5 | 0.530 | 0.22 |
| **Saddle_Shaped_Annulus_Perimeter (3D)** | (n=48) | (n=10) | (n=38) | | |
| Mean ± SD | 14.3 ± 1.7 | 14.6 ± 1.9 | 14.2 ± 1.7 | 0.545 | 0.22 |
| **D-Shaped_Annulus_Area (2D)** | (n=47) | (n=10) | (n=37) | | |
| Mean ± SD | 13.5 ± 3.3 | 14.1 ± 3.8 | 13.4 ± 3.3 | 0.580 | 0.20 |
| **D-Shaped_Annulus_Perimeter** | (n=47) | (n=10) | (n=37) | | |
| Mean ± SD | 13.3 ± 2.2 | 13.7 ± 1.8 | 13.1 ± 2.3 | 0.490 | 0.25 |
| **Annulus_Height** | | | | | |
| Mean ± SD | 1.00 ± 0.25 | 0.97 ± 0.24 | 1.01 ± 0.25 | 0.588 | -0.18 |
| **Non-planar_Angle** | | | | | |
| Mean ± SD | 144.0 ± 11.5 | 145.3 ± 10.6 | 143.6 ± 11.9 | 0.652 | 0.15 |
| **Tenting_Volume** | (n=31) | (n=5) | (n=26) | | |
| Median | 2.10 | 1.86 | 2.18 | 0.809 | -0.08 |
| (P25 – P75) | (1.58 – 3.60) | (1.14 – 3.42) | (1.59 – 3.60) | | |
| Minimum – maximum | 0.17 – 8.53 | 1.04 – 8.53 | 0.17 – 7.34 | | |
| **Coaptation_Depht** | (n=48) | (n=10) | (n=38) | | |
| Median | 9.2 | 7.1 | 10.6 | 0.676 | -0.09 |
| (P25 – P75) | (4.7 – 12.8) | (4.7 – 14.6) | (4.7 – 12.5) | | |
| Minimum – maximum | 0.5 – 19.5 | 1.7 – 19.5 | 0.5 – 16.3 | | |
| **Tenting_Area** | (n=44) | (n=10) | (n=34) | | |
| Median | 1.37 | 1.02 | 1.53 | **0.048** | -0.41 |
| (P25 – P75) | (1.02 – 1.98) | (0.67 – 1.31) | (1.17 – 2.13) | | |
| Minimum – maximum | 0.20 – 4.53 | 0.38 – 4.53 | 0.20 – 3.50 | | |
| **Angle_Aao-AP** | | | | | |
| Mean ± SD | 112.7 ± 10.9 | 112.5 ± 9.7 | 112.8 ± 11.3 | 0.933 | -0.03 |
| **Maximum_Prolapse_Height** | (n=46) | (n=10) | (n=36) | | |
| Median | 7.20 | 7.87 | 6.65 | 0.228 | **0.39** |
| (P25 – P75) | (3.68 – 8.86) | (6.95 – 8.86) | (3.65 – 8.82) | | |
| Minimum – maximum | 0.39 – 14.63 | 1.57 – 11.64 | 0.88 – 14.63 | | |
| **Maximal_Open_Coaptaiton_Gap** | (n=16) | (n=3) | (n=13) | | |
| Median | 1.76 | 0 | 2.11 | 0.721 | 0.18 |
| (P25 – P75) | (0 – 3.58) | (0 – 11.74) | (0.3 – 3.24) | | |
| Minimum – maximum | 0 – 11.74 | 0 – 11.74 | 0 – 5.63 | | |
| **Maximal_Open_Coaptation_Width** | (n=46) | (n=10) | (n=36) | | |
| Mean ± SD | 42.4 ± 7.9 | 42.8 ± 7.9 | 42.3 ± 8.3 | 0.842 | 0.07 |
| **Total_Open_Coaptation_Area (3D)** | (n=16) | (n=3) | (n=13) | | |
| Median | 0.17 | 0 | 0.19 | 0.721 | 0.18 |
| (P25 – P75) | (0 – 0.53) | (0 – 2.79) | (0.02 – 0.52) | | |
| Minimum – maximum | 0 – 2.79 | 0 – 2.79 | 0 – 0.97 | | |
| **Anterior_Leaflet_Area** | | | | | |
| Mean ± SD | 8.9 ± 2.4 | 9.5 ± 2.5 | 8.8 ± 2.3 | 0.346 | 0.31 |
| **Posterior_Leaflet_Area** | | | | | |
| Mean ± SD | 10.9 ± 3.4 | 12.7 ± 4.3 | 10.4 ± 2.9 | **0.031** | **0.74** |
| **Distal_Anterior_Leaflet_Angle** | | | | | |
| Mean ± SD | 19.7 ± 10.9 | 17.7 ± 11.1 | 20.3 ± 10.9 | 0.467 | -0.24 |
| **Posterior_Leaflet _Angle** | | | | | |
| Mean ± SD | 27.0 ± 15.4 | 23.7 ± 17.1 | 28.0 ± 14.9 | 0.395 | 0.28 |
| **Anterior_Leaflet_Lenght** | (n=50) | (n=12) | (n=38) | | |
| Mean ± SD | 2.89 ± 0.45 | 2.91 ± 0.55 | 2.89 ± 0.42 | 0.899 | 0.04 |

 doi:10.20944/preprints202601.0344.v1



| | | | | | |
|---|---|---|---|---|---|
| **Posterio_Leaflte_Lenght** | | | | | |
| Mean ± SD | 2.58 ± 0.56 | 2.88 ± 0.67 | 2.48 ± 0.50 | **0.032** | **0.73** |
| **Annulus_Area (2D)** | (n=50) | (n=12) | (n=38) | | |
| Mean ± SD | 14.8 ± 3.7 | 16.2 ± 4.2 | 14.3 ± 3.5 | 0.115 | **0.53** |
| **Anterior_Closure_Line_Lenght (2D)** | (n=49) | (n=12) | (n=37) | | |
| Mean ± SD | 4.10 ± 0.71 | 4.21 ± 0.72 | 4.07 ± 0.71 | 0.548 | 0.20 |
| **Anterior_Closure_Line_Lenght (3D)** | (n=49) | (n=12) | (n=37) | | |
| Mean ± SD | 4.26 ± 0.76 | 4.39 ± 0.77 | 4.22 ± 0.76 | 0.527 | 0.21 |
| **Posterior_Closure_Line_Lenght (2D)** | (n=49) | (n=12) | (n=37) | | |
| Mean ± SD | 4.10 ± 0.70 | 4.21 ± 0.72 | 4.06 ± 0.71 | 0.521 | 0.21 |
| **Posterior_Closure_Line_Lenght (3D)** | (n=49) | (n=12) | (n=37) | | |
| Mean ± SD | 4.26 ± 0.74 | 4.36 ± 0.72 | 4.22 ± 0.75 | 0.577 | 0.19 |
| **C-Shaped_Annulus** | (n=49) | (n=12) | (n=37) | | |
| Mean ± SD | 10.48 ± 1.37 | 10.90 ± 1.55 | 10.35 ± 1.30 | 0.226 | 0.41 |
| **Annular_Displacement (max)** | (n=49) | (n=12) | (n=37) | | |
| Mean ± SD | 9.96 ± 2.62 | 10.46 ± 2.81 | 9.80 ± 2.57 | 0.452 | 0.25 |
| **Annular_Displecement_Velocity (máx)** | (n=9) | (n=1) | (n=8) | | |
| Mean ± SD | 35.3 ± 9.0 | 51.3 | 33.3 ± 7.2 | - | - |
| **Tenting_Volume_Fraction** | (n=19) | (n=5) | (n=14) | | |
| Mean ± SD | 56.7 ± 24.2 | 50.4 ± 29.0 | 58.9 ± 23.0 | 0.515 | 0.35 |
| **Annulus_Area_Fraction (2D)** | (n=45) | (n=11) | (n=34) | | |
| Median | 7.6 | 6.7 | 7.6 | 0.700 | 0.08 |
| (P25 – P75) | (3.7 – 17.2) | (2.1 – 17.2) | (4.0 – 14.1) | | |
| Mínimo – máximo | 0.7 – 31.8 | 1.0 – 31.8 | 0.7 – 31.8 | | |

#. d-Cohen para teste t de Student ou δ de Cliff para teste de Mann-Whitney; A-P: anteroposterior; AL-PM: anteroposterior-posteromedial.

**Table 6.** New automatic software measures according to 75 percentile of regurgitant volume.

| Variable | Total (n=50) | Regurgitant volume | | p-Value | Effect Size # |
|---|---|---|---|---|---|
| | | ≥ 70 ml/beat (n=13) | < 70 ml/beat (n=37) | | |
| **AP Diameter** | | | | | |
| Mean ± SD | 4.21 ± 0.47 | 4.30 ± 0.50 | 4.17 ± 0.46 | 0.410 | 0.27 |
| **AL-PM_Diameter** | | | | | |
| Mean ± SD | 4.49 ± 0.58 | 4.62 ± 0.65 | 4.44 ± 0.57 | 0.361 | 0.30 |
| **Sphericity_Index (AP / AL-PM)** | | | | | |
| Mean ± SD | 0.94 ± 0.07 | 0.93 ± 0.05 | 0.94 ± 0.07 | 0.654 | -0.15 |
| **Commissural_Diameter** | | | | | |
| Mean ± SD | 4.37 ± 0.60 | 4.50 ± 0.69 | 4.32 ± 0.57 | 0.381 | 0.29 |
| **Saddle_Shaped_Annulus_Area (3D)** | (n=47) | (n=12) | (n=35) | | |
| Mean ± SD | 15.2 ± 3.6 | 15.7 ± 3.9 | 15.1 ± 3.6 | 0.632 | 0.16 |
| **Saddle_Shaped_Annulus_Perimeter (3D)** | (n=47) | (n=12) | (n=35) | | |
| Mean ± SD | 14.3 ± 1.7 | 14.5 ± 1.9 | 14.2 ± 1.7 | 0.626 | 0.16 |
| **D-Shaped_Annulus_Area (2D)** | (n=46) | (n=12) | (n=34) | | |
| Mean ± SD | 13.5 ± 3.4 | 13.8 ± 3.7 | 13.4 ± 3.3 | 0.727 | 0.12 |
| **D-Shaped_Annulus_Perimeter** | (n=46) | (n=12) | (n=34) | | |
| Mean ± SD | 13.3 ± 2.2 | 13.6 ± 1.8 | 13.1 ± 2.3 | 0.555 | 0.20 |
| **Annulus_Height** | | | | | |

 doi:10.20944/preprints202601.0344.v1



| | | | | | |
|---|---|---|---|---|---|
| Mean ± SD | 1.00 ± 0.25 | 0.99 ± 0.28 | 1.00 ± 0.24 | 0.882 | -0.05 |
| **Non-planar_Angle** | | | | | |
| Mean ± SD | 144.0 ± 11.6 | 144.7 ± 11.0 | 143.7 ± 12.0 | 0.796 | 0.08 |
| **Tenting_Volume** | (n=30) | (n=6) | (n=24) | | |
| Median | 2.00 | 2.64 | 2.00 | 0.699 | 0.11 |
| (P25 – P75) | (1.58 – 3.42) | (1.16 – 4.06) | (1.59 – 3.08) | | |
| Minimum – maximum | 0.17 – 8.53 | 1.14 – 8.53 | 0.17 – 7.34 | | |
| **Coaptation_Depht** | (n=47) | (n=12) | (n=35) | | |
| Median | 9.1 | 7.1 | 10.6 | 0.458 | -0.15 |
| (P25 – P75) | (4.7 – 12.5) | (3.2 – 12.4) | (4.7 – 12.5) | | |
| Minimum – maximum | 0.5 – 19.5 | 1.7 – 19.5 | 0.5 – 15.5 | | |
| **Tenting_Area** | (n=43) | (n=10) | (n=33) | | |
| Median | 1.36 | 1.02 | 1.40 | 0.206 | -0.27 |
| (P25 – P75) | (1.02 – 1.96) | (0.66 – 1.81) | (1.17 – 1.96) | | |
| Minimum – maximum | 0.20 – 4.53 | 0.38 – 4.53 | 0.20 – 3.50 | | |
| **Angle_Aao-AP** | | | | | |
| Mean ± SD | 112.6 ± 10.9 | 112.4 ± 9.3 | 112.6 ± 11.5 | 0.954 | -0.02 |
| **Maximum_Prolapse_Height** | (n=45) | (n=12) | (n=33) | | |
| Median | 7.44 | 7.87 | 6.85 | 0.408 | 0.17 |
| (P25 – P75) | (3.85 – 8.86) | (4.02 – 8.86) | (3.65 – 8.77) | | |
| Minimum – maximum | 0.88 – 14.63 | 1.57 – 11.64 | 0.88 – 14.63 | | |
| **Maximal_Open_Coaptaiton_Gap** | (n=16) | (n=3) | (n=13) | | |
| Median | 1.76 | 0 | 2.11 | 0.721 | -0.18 |
| (P25 – P75) | (0 – 3.58) | (0 – 11.74) | (0.3 – 3.24) | | |
| Minimum – maximum | 0 – 11.74 | 0 – 11.74 | 0 – 5.63 | | |
| **Maximal_Open_Coaptation_Width** | (n=45) | (n=12) | (n=33) | | |
| Mean ± SD | 42.4 ± 8.0 | 42.6 ± 6.3 | 42.4 ± 8.6 | 0.923 | 0.03 |
| **Total_Open_Coaptation_Area (3D)** | (n=16) | (n=3) | (n=13) | | |
| Median | 0.17 | 0 | 0.19 | 0.721 | -0.18 |
| (P25 – P75) | (0 – 0.53) | (0 – 2.79) | (0.02 – 0.52) | | |
| Minimum – maximum | 0 – 2.79 | 0 – 2.79 | 0 – 0.97 | | |
| **Anterior_Leaflet_Area** | | | | | |
| Mean ± SD | 8.9 ± 2.4 | 9.3 ± 2.2 | 8.8 ± 2.4 | 0.520 | 0.21 |
| **Posterior_Leaflet_Area** | | | | | |
| Mean ± SD | 10.9 ± 3.4 | 12.0 ± 4.3 | 10.5 ± 3.0 | 0.186 | 0.43 |
| **Distal_Anterior_Leaflet_Angle** | | | | | |
| Mean ± SD | 19.5 ± 10.9 | 16.3 ± 10.1 | 20.6 ± 11.0 | 0.221 | 0.40 |
| **Posterior_Leaflet _Angle** | | | | | |
| Mean ± SD | 26.7 ± 15.3 | 23.9 ± 18.0 | 27.6 ± 14.4 | 0.458 | -0.24 |
| **Anterior_Leaflet_Lenght** | (n=49) | (n=13) | (n=36) | | |
| Mean ± SD | 2.88 ± 0.45 | 2.94 ± 0.50 | 2.86 ± 0.43 | 0.630 | 0.16 |
| **Posterio_Leaflte_Lenght** | | | | | |
| Mean ± SD | 2.58 ± 0.57 | 2.77 ± 0.64 | 2.51 ± 0.53 | 0.159 | 0.46 |
| **Annulus_Area (2D)** | (n=49) | (n=13) | (n=36) | | |
| Mean ± SD | 14.8 ± 3.7 | 15.7 ± 4.2 | 14.4 ± 3.6 | 0.299 | 0.34 |
| **Anterior_Closure_Line_Lenght (2D)** | (n=48) | (n=13) | (n=35) | | |
| Mean ± SD | 4.11 ± 0.71 | 4.20 ± 0.69 | 4.07 ± 0.73 | 0.598 | 0.17 |
| **Anterior_Closure_Line_Lenght (3D)** | (n=48) | (n=13) | (n=35) | | |
| Mean ± SD | 4.27 ± 0.77 | 4.34 ± 0.74 | 4.24 ± 0.79 | 0.705 | 0.12 |
| **Posterio_Closure_Line_Lenght (2D)** | (n=48) | (n=13) | (n=35) | | |
| Mean ± SD | 4.10 ± 0.71 | 4.20 ± 0.69 | 4.07 ± 0.73 | 0.579 | 0.18 |
| **Posterior_Closure_Line_Lenght (3D)** | (n=48) | (n=13) | (n=35) | | |
| Mean ± SD | 4.26 ± 0.75 | 4.31 ± 0.69 | 4.24 ± 0.78 | 0.775 | 0.09 |

 doi:10.20944/preprints202601.0344.v1



| | | | | | |
|---|---|---|---|---|---|
| **C-Shaped_Annulus** | (n=48) | (n=13) | (n=35) | | |
| Mean ± SD | 10.48 ± 1.38 | 10.64 ± 1.54 | 10.42 ± 1.34 | 0.625 | 0.16 |
| **Annular_Displacement (max)** | (n=48) | (n=13) | (n=35) | | |
| Mean ± SD | 10.02 ± 2.61 | 10.01 ± 3.37 | 10.02 ± 2.33 | 0.982 | -0.01 |
| **Annular_Displecement_Velocity (máx)** | (n=9) | (n=3) | (n=6) | | |
| Median | 31.6 | 38.9 | 30.4 | 0.905 | 0.11 |
| (P25 – P75) | (28.5 – 39.6) | (25.5 – 51.3) | (28.5 – 39.6) | | |
| Minimum – maximum | 25.5 – 51.3 | 25.5 – 51.3 | 27.3 – 45.8 | | |
| **Tenting_Volume_Fraction** | (n=18) | (n=5) | (n=13) | | |
| Mean ± SD | 56.4 ± 29.8 | 51.4 ± 29.8 | 58.3 ± 23.8 | 0.616 | -0.27 |
| **Annulus_Area_Fraction (2D)** | (n=44) | (n=13) | (n=31) | | |
| Median | 7.5 | 6.7 | 7.6 | 0.934 | -0.02 |
| (P25 – P75) | (3.6 – 17.2) | (2.3 – 17.2) | (3.8 – 14.1) | | |
| Minimum – maximum | 0.7 – 31.8 | 0.9 – 31.8 | 0.7 – 31.8 | | |

#. d-Cohen para teste t de Student ou δ de Cliff para teste de Mann-Whitney. A-P: anteroposterior; AL-PM: anteroposterior-posteromedial.

Intraclass correlation coefficient (ICC) for intra-observer variability was >0.96 for all variables for MVP and PFO patients with coefficient of variation < 1.2%. For inter-observer variability, ICC was >0.95, with coefficient of variation < 1.7%. for all variables for MVP and PFO patients.

## 4. Discussion

The main finding of this manuscript is that twenty-seven automatic parameters (79%) wefe different concerning MVP and patients without cardiac chambers alterations (PFO patients) ($p<0.05$): anteroposterior anular diameter, anterolateral-postromedial diameter, commissural diameter, saddle shaped annulus area (3D), saddle shaped annulus perimeter (3D), D-shaped annulus area (2D), D-shaped annulus perimeter, annulus height, non-planar angle, maximal open coaptation width, anterior leaflet area, posterior leaflet area, anterior leaflet lenght, posterior leaflt lenght, annulus area (2D), anterior closure line lenght (2D), anterior closure line lenght (3D), posterior closure line lenght (2D), posterior closure line lenght (3D), C-shaped annulus ($p<0.05$). Other two parameters (5%), tenting area and annular displacement velocity max, were marginally different concerning groups (both p: 0.052), The effect sizes (Hedges' g between 1.0 and 2.0) indicate very large differences. with 95% CIs far from zero, reflecting annular remodeling and global enlargement of the valve apparatus in cases of MI. These differences suggest significant dilatation of the annulus and valve leaflets, consistent with the pathophysiology of degenerative mitral regurgitation.

The variable maximum prolapse height was not normally distributed, but through the Mann-Whitney test it was possible to verify that patients with MVP had a statistically higher median Maximum Prolapse Height than that presented by patients with PFO ($p<0.001$), with a very large effect size ($g=4.22$; 95%CI 2.69–6.40), corroborating the greater degree of leaflet prolapse.

The combination of clinically relevant absolute differences (0.6–1.0 cm in principal diameters) and very large effect sizes (Hedges' g > 1.5) supports the clinical relevance of the anatomical discrepancies identified by the automatic software, regardless of the absence of prior sample size calculation.

The mean ERO (0.42 $cm^2$) and mean regurgitant volume (62.9 mL/beat) were close to levels considered to represent patients with important mitral valve regurgitation. In this sense, we choosed to correlate the use of the automatic software in the subgroup of patients in the 75 percentile of ERO and regurgitant volume, what could represent patients with more advanced MVP. In this sense we tested the software in patients with ERO >0.48 $cm^2$ and regurgitant volume > 70 ml/beat. According to Table 5, it can be observed that there was a statistically significant effect with a moderate to important effect size for the variables: posterior leaflet area, posterior leaflet length and tenting area.

 doi:10.20944/preprints202601.0344.v1



Posterior leaflet area showed statistically higher mean values among patients with ERO ≥ 0.48 cm² when compared to those with ERO < 0.48 cm² (mean difference = 2.39 ± 1.07; CI95: 0.23 to 4.54; p=0.031 and moderate to important effect size: d=0.74). Clinically, it can be interpreted that a larger posterior leaflet area was associated with elevated ERO. In the same way, posterior leaflet length showed a statistically higher mean in the ERO ≥ 0.48 cm² group when compared with those with ERO < 0.48 cm² (mean difference = 0.40 ± 0.18; CI95: 0.04 to 0.75; p=0.032 and moderate to important effect size: d=0.73). Thus, a longer posterior cusp was observed in patients with greater regurgitation. Also, tenting area presented an asymmetric distribution and was smaller among patients with ERO ≥ 0.48 cm² (median 1.02; P25=0.67 and P75=1.31) versus (median 1.53; P25=1.17 and P75=2.13); p=0.048; moderate effect size: =0.41). That is, smaller tenting area values were observed in the ERO ≥ 0.48 cm² group. Clinically, this pattern was compatible with a prolapsing/degenerative phenotype (smaller tenting area) in cases with higher ERO.

According to Table 6, it can be observed that there was no statistically significant effect on any of the variables of the new software according to P75 of the regurgitation volume (p>0.05). Even so, small effect sizes suggest a morphofunctional pattern compatible with a primary valve mechanism (degenerative/prolapsing) in the regurgitation volume group with values greater than or equal to P75. Also, the set of data consistently points in the direction (even without p<0.05) of a primary valve phenotype in cases with RV≥70 ml/btm: larger/longer posterior cusp and smaller tenting/coaptation depth. The slightly larger annulus appears as a trend, without statistical proof in this sample. In summary, the pattern favors a degenerative/prolapse mechanism as reason for mitral valve changes.

Previous studies have adressed tridimensional echocardiography softwares dedicated to mitral valve apparatus analysis 6,8, 16,17,18,19,20. They brought important information concerning mitral annulus 8, distance from posteromedial pappilary muscles to mitral valve edge what can bring implications to good results for surgical repair 11.

Mitral valve repair, first described by Carpentier 56 years ago 15, remains the gold standard for treating degenerative mitral regurgitation. Recent advances in minimally invasive and robotic cardiac surgery aim to enhance the safety and efficacy of mitral valve repair 13. In this setting, the development of automated echocardiographic software tools may further improve reproducibility and standardization of the procedure, supporting its wider adoption in clinical practice. We believe that our investigation could bring and add new information concerning automatic mitral valve analysis and eventual useful information for surgical treatment. The efficiency, accuracy and potencial use of the coming mitral valve apparatus analysis softwares are to be validaded in future investigations 15-20.

## 5. Limitations

This investigations concerns a small sample single center mitral valve prolapse patients with moderate and severe mitral regurgitation from a tertiary Brazilian hospital. Our results have to be validated in a higher population sample envolving multiple centers in different countries.

## 6. Conclusions

Automatic mitral valve parameters analysis were different concerning MVP and no structural cardiac chamber (PFO) patients. 75 percentile ERO MVP patients (ERO> 0.48 cm²) correlated to posterior leaflet parameters. This anatomic information could be useful to planning and surgical treatment of mitral valve prolapse patients.

**Author Contributions:** Conceptualization, MLCV, ACTR., ED; Methodology, MLCV, ACL, ACTR, RP, WO.; Validation, ED, AR, AACL, GPA, AJO, LOAS, RACM, RP, .; Formal Analysis, GPA, CGM, MLCV, LOAS, RACM, AS; Investigation, SSM, CHF, EBLF, AJO, SOC; Writing – Original Draft Preparation, MLCV, CHF, SSM, ED, RBP, FAS, FOO,WO .; Writing – Review & Editing, MLCV, CHF, SSM, ED, RBP, FAS, FOO,WO .; Visualization, MLCV, CHF, SSM, ED, RBP, FAS, FOO,WO.; Supervision, MLCV, CHF, SSM, ED, RBP, FAS, FOO,WO.

 doi:10.20944/preprints202601.0344.v1



**Funding:** This research received no external funding.

**Informed Consent Statement:** Informed consent was obtained from all subjects involved in the study.

**Data Availability Statement:** The original contributions presented in this study are included in the article/supplementary material. Further inquiries can be directed to the corresponding author.

**Conflicts of Interest:** The authors declare no conflict of interest.

## References

1. Agricola E. Francesco A. Bartel T. Brochet E. Marc D. Faletra F. et al Multimodality imaging for patient selection. procedural guidance. and follow-up of transcatheter interventions for structural heart disease: a consensus document of the EACVI Task Force on Interventional Cardiovascular Imaging: part 1: access routes. transcatheter aortic valve implantation. and transcatheter mitral valve interventions. Eur Heart J Cardiovasc Imaging 2023;24 (9): e209–e268.
2. Faletra F. et al. The structural heart disease interventional imager rationale. skills and training: a position paper of the European Association of Cardiovascular Imaging. Eur Heart J Cardiovasc Imaging. 2021;22(5):471-479.
3. Vahanian A. Beyersdorf F. Praz F. Milojevic M. Baldus S. Bauersachs J. et al. ESC/EACTS Scientific Document Group. 2021 ESC/EACTS guidelines for the management of valvular heart disease. Eur Heart J 2022;43(7):561-632.
4. Nishimura RA. Vahanian A. Eleid MF. Mack MJ. Mitral valve disease— current management and future challenges. Lancet. 2016;387:1324–1334.
5. Gammie JS. O'Brien SM. Griffith BP. Ferguson TB. Peterson ED. Influence of hospital procedural volume on care process and mortality for patients undergoing elective surgery for mitral regurgitation. Circulation. 2007;115:881–887.
6. Calleja A, Poulin F, Woo A, et al. Quantitative modeling of the mitral valve by three-dimensional transesophageal echocardiography in patients undergoing mitral valve repair: correlation with intraoperative surgical technique. J Am Soc Echocardiogr. 2015;28:1083–92.
7. Melamed T Badiani . Harlow S. Laskar N. Treibel T. Aung N. et al Prevalence. progression. and clinical outcomes of mitral valve prolapse: a systematic review and meta-analysis. Eur Heart J Qual Care Clin Outcomes 2025 ;11(5):631-641.
8. Berthelot-Richer M , Vakulenko H V, Calleja A, Woo A, Paaladinesh Thavendiranathan P, Poulin F. Two-dimensional transthoracic measure of mitral annulus in mitral valve prolapse and moderate to severe regurgitation: a method comparison analysis with three-dimensional transesophageal echocardiography. J Cardiovasc Imaging. 2024 Jun 12;32(1):2
9. Nishimura RA, Otto CM, Bonow RO, et al. 2014 AHA/ACC guideline for the management of patients with valvular heart disease: a report of the American College of Cardiology/American heart association task force on practice guidelines. J Am Coll Cardiol. 2014;63:e57-185.
10. Clavel MA, Mantovani F, Malouf J, et al. Dynamic phenotypes of degenerative myxomatous mitral valve disease: quantitative 3-dimensional echocardiographic study. Circ Cardiovasc Imaging. 2015;8:e002989.
11. Pardi MM , Pomerantzef PMA, Sampaio RO, Abduch MA, Brandão CMA, Mathias Jr W, et al. Relation of mitral valve morphology to surgical repair results in patients with mitral valve prolapse: A three-dimensional transesophageal echocardiography study. Echocardiography . 2018;35(9):1342-1350.
12. Guedes MA, Pomerantzeff PM, Brandão CM, Vieira ML, Tarasoutchi F, et al. Mitral annulus morphologic and functional analysis using real time tridimensional echocardiography in patients submitted to unsupported mitral valve repair. Rev Bras Cir Cardiovasc. 2015 ;30(3):325-34.
13. Poffo R, Toschi AP, Pope RB, Montanhesi PK, Santos RS, Teruya A, et al. Ann Cardiothorac Surg. 2017 Jan;6(1):17-26.
14. Lang RM, Badano LP, Mor-Avi V, et al. Recommendations for cardiac chamber quantification by echocardiography in adults: an update from the American Society of Echocardiography and the European Association of Cardiovascular Imaging. J Am Soc Echocardiogr. 2015;28:1-39.e14.

 doi:10.20944/preprints202601.0344.v1



15. Carpentier A. Reconstructive valvuloplasty: A new technique of mitral valvuloplasty. Presse Med. 1969;77(27):251–3.
16. Wifstad SV, Kildahl HA, Grenne B, Estensen ME · Dalen H · Lovstakken L. Mitral Valve Segmentation and Tracking from Transthoracic Echocardiography Using Deep Learning. Ultrasound Med Biol . 2024;50(5):661-670.
17. Messika-Zeitoun D , Theriault-Lauzier , Burwash IG. Diagnosis of Mitral Valve Prolapse Using Artificial Intelligence: Is it Ready for Primetime? JACC Cardiovasc Imaging . 2025 29:S1936-878X(25)00514-5.
18. Wu Z, Ge Z, Ge Z, Xing Y, Zhao W, Dong L, et al. Feasibility validation of automatic diagnosis of mitral valve prolapse from multi-view echocardiographic sequences based on deep neural network. Eur Heart J Imaging Methods Pract . 2024;2(4):qyae086.
19. Al-Alusi MA, Lau ES, Small AM, Reeder C, Shnitzer T, Andrews CT, et al. A Deep Learning Model to Identify Mitral Valve Prolapse From the Echocardiogram. JACC Cardiovasc Imaging 2025:S1936-878X(25)00474-7.
20. Vafaeezadeh M1, Behnam H, Hosseinsabet A, Gifani P. Automatic morphological classification of mitral valve diseases in echocardiographic images based on explainable deep learning methods. Int J Comput Assist Radiol Surg . 2022;17(2):413-425.